Journal of Wind Engineering & Industrial Aerodynamics 199 (2020) 104118

Contents lists available at ScienceDirect

Journal of Wind Engineering & Industrial Aerodynamics

journal homepage: www.elsevier.com/locate/jweia

Combination of wind gust models in convective events

Alejandro Gutiérrez [a,*], Claudio Porrini [a], Robert G. Fovell [b]

[a] Instituto de Mecánica de los Fluidos e Ingeniería Ambiental, Facultad de Ingeniería, Universidad de la República, Montevideo, Uruguay
[b] Atmospheric and Environmental Sciences, University at Albany, State University of New York, United States

ARTICLE INFO

Keywords:
Wind energy
Forecast
Gust

ABSTRACT

Gusts are particularly relevant to wind engineering and it is of interest to develop a forecasting tool for wind energy management for systems such as Uruguay's, which has a wind power participation of 38% (UTE, 2019). In the present work, we assess the performance of two gust parameterizations (Gutiérrez–Fovell and Nakamura et al.) utilizing Weather Research and Forecasting (WRF) model simulations for predicting gusts at 100 m above ground level in the presence of convection. Convective activity is predicted when the vertically accumulated rain water mixing ratio computed by the model exceeds a selected value and is verified in part via satellite imagery (GOES-13). Gust forecast skill is evaluated with wind tower observations. We find a combination of the two parameterizations yields the highest forecast skill.

1. Introduction

Wind gusts represent the maximum wind speed observed over a fixed period, and reliable gust forecasts can potentially mitigate the destruction they can cause (Friederichs et al., 2009). Gusts are relevant to wind energy production, particularly in systems such as Uruguay's in which wind power has a participation of 38% (UTE, 2019). Gusts are more likely to occur in some weather regimes than others. For example (Hu et al., 2018), have analyzed observational data from 3D sonic anemometers in a moderately complex terrain at near wind turbine heights, and found that large gust length scales and gust factors are more likely to be observed in unstable atmospheric conditions. In apparent contrast (Gutiérrez and Fovell, 2018), discovered that large gusts measured by turbine height sonic anemometers were much more likely to occur when the lapse rate between the tower base and top was neutral. In that study, thermometers located near tower base (ranging from 2 to 12 m above) and ~100 m were employed. Additionally, gusts also have a large degree of subregional variability (e.g., Letson et al., 2018) and can also vary significantly with height (Beljaars, 1987).

Gusts represent turbulent activity and their generation and impacts on structures such as wind turbines and aircraft can be studied with very high-resolution "large eddy simulation" models (e.g., Knigge and Raasch, 2016), albeit at high computational cost. A more economical approach is to use mesoscale weather prediction models but the energy-containing turbulent eddies involved in gustiness are usually far too small to be resolved (Wyngaard, 2004) and, as a consequence, gusts have to be parameterized in some fashion. A variety of gust parameterizations have been employed, ranging from simple (e.g., Cao and Fovell, 2018) to more complex, some being developed for very specific applications (e.g., Yang and Tsai, 2019 for tropical cyclones). (Gutiérrez and Fovell, 2018) created a gust parameterization for wind energy applications utilizing information provided by the Weather Research and Forecasting (WRF) model (Skamarock and co-authors, 2008), and evaluated it with observations collected in Uruguay's network of wind towers.

The (Gutiérrez and Fovell, 2018) scheme was shown to have some skill in anticipating potentially damaging winds, although its success was dependent on WRF model forecast skill and evinced sensitivity to model physical parameterizations. In addition, the scheme was developed primarily with *non-convective* gusts in mind. It is well appreciated that convective storms can generate large wind bursts (cf., Choi and Hidayat, 2002; Shu et al., 2015). Convective activity is frequent in South America (Zipser et al., 2006) and mesoscale convective systems (MCSs) such as supercell and multicell storms are commonly observed (Mulholland et al., 2018). Storm intensity is closely related to convective mode (Dial et al., 2010). (Brooks et al., 2003) have discussed the dynamics driving the development of convective storms in the subtropical South American region, which include cyclogenesis near the Andes mountains as well as low-level humidity transported by the South America Low Level Jet (SALLJ) (Virji, 1981; Paegle et al., 1987; Vera et al., 2006), a strong wind blowing from the Amazonian jungle to low latitudes. Many studies have

* Corresponding author.
E-mail address: aguti@fing.edu.uy (A. Gutiérrez).
URL: http://www.fing.edu.uy (A. Gutiérrez).

https://doi.org/10.1016/j.jweia.2020.104118
Received 3 October 2019; Received in revised form 30 January 2020; Accepted 30 January 2020
Available online xxxx
0167-6105/

suggested an active role for the SALLJ in the positioning and intensity of the South Atlantic convergence zone and the rainfall and convection at the exit region of the jet in southeastern South America (e.g., Mo and Paegle, 2001; Berbery and Collini, 2001; Cazes-Boezio et al., 2003; Saulo et al., 2004; Marengo et al., 2004). Also, many studies (e.g., Nesbitt el al., 2006; Zipser et al., 2006; Rasmussen and Houze, 2011) have employed satellite images to detect and analysis convective systems in South America.

For all gust models, adequate performance requires skillful predictions of the input parameters, which may include mean (sustained) winds, boundary layer depths, vertical stabilities, and hydrometeor fields, among many others. Regarding winds in particular (Stucki et al., 2016), reported that the WRF model tended to overpredict the mean wind, while (Cao and Fovell, 2016, 2018), which utilized a dense mesonet to verify winds and gust forecasts during "Santa Ana" windstorms, have demonstrated that this can be dependent on the land surface model (LSM) employed, owing to its specification of surface roughnesses. Clouds are inherently involved in convective gusts, which develops on time scales from minutes to hours and can produce strong vertical air currents. Considerable sensitivity to cumulus and/or microphysical parameterizations can therefore be anticipated.

The present work assesses the performance of the (Gutiérrez and Fovell, 2018) approach during likely convective events, with the aim of extending or modifying the parameterization to account for this important source of gusts. A variety of ways of specifically handling convective gusts have been explored in the literature. For example (Gray, 2003), used an algorithm to predict the maximum gust utilizing cloud top height, cloud depth, and virtual potential temperature, while the (Nakamura et al., 1996) approach incorporated presumed downdraught depth along with precipitation mixing ratio. We have elected to assess the performance of the latter, separately and in combination with our non-convective gust model, on potentially convective events that were identified via satellite images from a Geostationary Operational Environmental Satellite (GOES). As in (Gutiérrez and Fovell, 2018), information from WRF simulations will be used to predict gusts that will be compared to data recorded at a set of towers representing Uruguay's various regions.

The structure of this paper is as follows: in Section 2, the observational data used for this work is summarized, followed by a description of the WRF experiments in Section 3. Section 4 discusses the gust models we consider. Section 5 presents patterns of convection in the analyzed region and the methodology for discriminating likely convective cases is developed. The performance of the gust models in the likely convective cases is assessed in Section 6. Conclusions are presented in Section 7.

2. Observational data

2.1. Wind velocity observational data

In this work, wind velocity observations recorded at wind towers operated by UTE (the Administración Nacional de Usinas y Transmisiones Eléctricas) in Uruguay, collected to assess wind energy resources, were used to evaluate gust models. Uruguay's orography is dominated by low, rolling plains and sierras (with elevations not exceeding 500 m above mean sea level) and the five towers considered herein represent distinct geographical regions: Colonia Eulacio (CE), Jose Ignacio (JI), McMeekan (MM), Rosendo Mendoza (RM), and Valentines (VA); see Fig. 1. Each tower is equipped with two anemometers mounted orthogonally to filter the effect of the tower wake and installation, in adherence with IEC standard 61400–12 (IEC, 1988).

The wind measurements were performed with cup anemometers (NRG Systems 40, with a distance constant of 3 m) mounted at various heights, including turbine level, ~100 m above ground level (AGL). Gusts were determined from 2-s samples (0.5 Hz being the sampling frequency) and the mean (sustained) winds averaged these samples over 10-min intervals. Table 1 describes the measurements considered in this work.

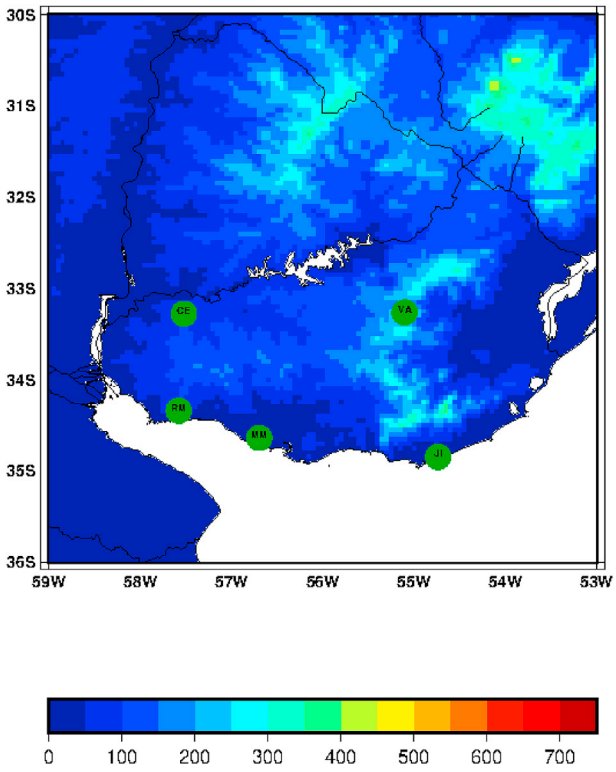

Fig. 1. Topographic map indicating locations of towers from which observational data were measured. See also Table 1.

Table 1
Tower locations, and heights of wind velocity measurements.

	Lat	Lon	Identifier	Anemometer height (m)
Colonia Eulacio	−33.280	−57.522	CE	101
Jose Ignacio	−34.850	−54.735	JI	98.4
McMeekan	−34.643	−56.695	MM	101.5
Rosendo Mendoza	−34.343	−57.578	RM	101.2
Valentines	−33.265	−55.101	VA	91.7

The analysis period was from 01/06/2016 to 31/05/2018, inclusive.

2.2. GOES satellite images

GOES provides high temporal resolution of cloud movement and evolution, which are useful to study and understand mesoscale atmospheric processes. The images from GOES-13 (East) cover South America with several channels. The infrared (IR) channel between 10 and 13 μm senses energy emitted by atmosphere, clouds, and the earth's surface. These images can provide cloud top temperature so that cloud top height can be inferred. The coldest cloud tops can help determine the areas where convection and extreme events occur. Images from these satellites are provided approximately every 30 min and the horizontal resolution is 4 km.

3. Numerical model and methods

Numerical simulations with WRF version 3.9, initialized using Global Forecasting System (GFS) operational product one-degree, 3-hourly of time step resolution, and employing three telescoping grids with horizontal resolutions of 30, 10, and 3.3 km (Fig. 2), were performed for the purpose of generating surface and boundary layer information for the gust parameterization models. The domain is centered on Uruguay and utilized MODIS topography and landuse information 36-h simulations

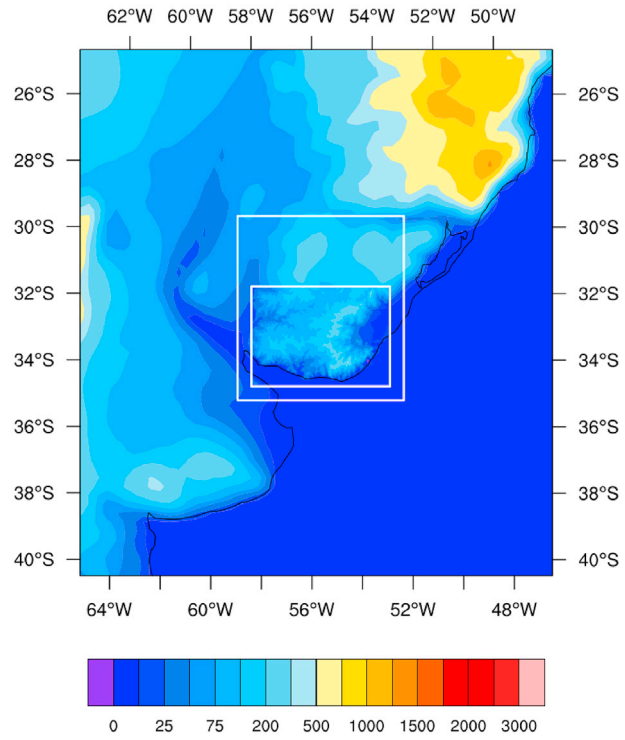

Fig. 2. WRF telescoping domain setup for simulations employed herein, showing model topography in meters. Horizontal grid spacings are 30, 10, and 3.3 km.

were initiated daily at 00 UTC spanning a period of two years from (01/06/2016 to 31/05/2018) with the first 12 h of each run discarded as spinup. As in (Gutiérrez and Fovell, 2018), the lowest model level is about 10 m AGL, while hub height (about 100 m) corresponds to the third model level above the surface.

Common model physics selections included the RRTM longwave (Mlawer et al., 1997) and Dudhia shortwave Dudhia (1989) radiation schemes, Lin microphysics (Lin et al., 1983), and the Noah land surface model (Chen and Dudhia, 2001). The Kain–Fritsch (Kain, 2004; Kain and Fritsch, 1990) cumulus parameterization was employed in the 30 km and 10 km domains, and gust model performance was assessed using two different PBL schemes, those being MYJ (Mellor and Yamada, 1974, 1982; Janjic, 1994), and Bretherton-Park (Bretherton and Park, 2009), both employing the MYJ surface layer scheme. MYJ is used in operational models at the National Centers for Environmental Prediction (NCEP) and Bretherton-Park performed well in the (Gutiérrez and Fovell, 2018) study.

4. Gust parameterizations

4.1. Gutiérrez and Fovell gust model

(Gutiérrez and Fovell, 2018) described a wind gust parameterization that comprises a first-guess gust factor (*GF*) that is subsequently modified under particularly favorable conditions. The first-guess *GF* consists of a minimum value (GF_{min}) augmented by a stability-dependent function of the model-predicted winds at and above the hub ($\approx$ 100 m) height, given by

$$GF = GF_{min} + K\frac{\Delta V^{Top}}{V_{100}}, \quad (1)$$

where K is a slope, V_{100} is the wind speed forecasted at hub height, and $\Delta V^{Top} = \max(0, V_{MAX} - V_{100})$ is a vertical speed difference. V_{MAX} is generally taken to be the wind speed at the PBL top, except under strongly stable temperature (T) conditions (i.e., $\frac{dT}{dz} \geq 0$, computed with temperatures at 100 m and 2 m of height), in which the wind at 200 m (twice the hub height) is used instead.

As discussed in (Gutiérrez and Fovell, 2018), parameters GF_{min} and K were determined for each tower separately via least squares, utilizing year-long WRF simulations, and permitted to vary with hub-height wind speed and vertical stability. Sensitivity to model physics and resolution was also detected. Fig. 3 presents the best-fit coefficients computed from this study's 3.3-km simulations employing the MYJ and Bretherton–Park schemes valid for the VA tower. Similar to (Gutiérrez and Fovell, 2018; see their Fig. 16), both GF_{min} and K were found to decrease with wind speed, and be sensitive to stability. The best fits obtained for the other towers were qualitatively quite similar (not shown) (Gutiérrez and Fovell, 2018). found that this formulation tended to underpredict particularly large gusts, for which they compensated by multiplying the predicted GF by an empirically-derived value ($S_{Ri} = 1.15$) when the anticipated gust exceeded 11.5 m/s and the surface layer stability was near-neutral. This refinement was employed in this study as well.

4.2. Nakamura gust model

(Nakamura et al., 1996) (hereafter "Nakamura") proposed a gust model for thunderstorms and for convection, using an energy conservation argument involving the processes that affect a parcel of air of mass m at height H that is about to become part of a convective downdraught. The parcel is moving horizontally with speed $V(H)$, having an initial kinetic energy $\frac{1}{2}mV(H)^2$. Precipitation falling into the parcel may evaporate (or melt), causing the parcel to cool, and this together with the loading effect of the precipitation itself gives the parcel negative buoyancy, causing it to accelerate downwards. Given the downward force on the parcel is $mg\Delta\theta/\theta + mgq_r$, where $\Delta\theta$ is the potential temperature deficit in the downdraught, θ is the potential temperature of the surroundings, and q_r, is the rain mixing ratio in the downdraught, the gust may be computed as

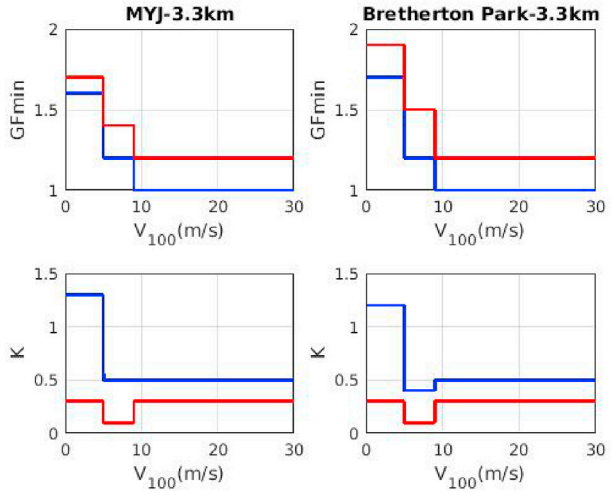

Fig. 3. Optimal fits of Gutiérrez and Fovell gust model parameters K and GF_{min} vs. hub-height wind speed V_{100} from VA tower observations and simulations using the MYJ and Bretherton–Park schemes with horizontal grid resolutions of 3.3 km during the training period from 01/06/2016 to 31/05/2017. Blue lines represent $\frac{\partial T}{\partial z} \geq 0$ and red represents $\frac{\partial T}{\partial z} < 0$, computed from the simulations. Hub-height velocity intervals applied to WRF forecasts were 0 m/s $< V_{100} \leq$ 5 m/s, 5 m/s $\leq V_{100} <$ 9 m/s and 9 m/s $\leq V_{100}$. When conditions indicated, the S_{Ri} adjustment was employed in these and all $G - -F$ forecasts in this study. (For interpretation of the references to colour in this figure legend, the reader is referred to the Web version of this article.)

$$V_{gust} = \sqrt{\alpha \int_0^H 2g\left(\frac{\Delta\theta}{\theta} + q_r\right) dz + \beta V(H)^2}. \quad (2)$$

The two terms on the right hand side represent buoyancy production and downward transport of momentum, respectively. The tunable parameters (α and β) were introduced by (Nakamura et al., 1996) to adjust the contributions of the two terms based on available model information and assumptions.

The Nakamura model is intended to capture gusts associated with thunderstorms and extratropical cyclones, so in an operational model a trigger is needed to identify convective activity. In our application, we activate their scheme *only* when $q_r^a \geq 0.0003$ kg_{H2O}/kg_{air}, where q_r^a is the column-integrated rainwater mixing ratio. For the classification of convective activity we employed GOES satellite images to help filter out false positives, including light or stratiform rain situations, from truly convective events, and this helped lead us to the empirically selected q_r^a threshold . As noted by Nakamura, (2) is very sensitive to H, which we specify as the height above the ground possessing descending motion, enforcing minimum and maximum values of 100 and 2000 m, respectively. $\Delta\theta$, the downdraught buoyancy deficit, is taken as the surface potential temperature decrease for each grid box from the previous hour, bounded from above by zero. This is roughly similar to Nakamura's approach in their idealized simulations, and does not explicitly filter out the diurnal cycle. Based on the results of (Nakamura et al., 1996), however, we anticipate that the buoyancy term in (2) is of relatively lesser importance. Two full years of simulations provided a sufficient number of cases (tabulated in Table 2) to permit reasonable estimations for the parameters α and β (Table 3) for our application.

Similar values of α and β were obtained by both PBLs schemes, in comparison with those reported by (Nakamura et al., 1996), instead of the qualitative difference of the numerical experiment, and number of cases considered in the present work.

Both the G–F and Nakamura parameterizations depend on coefficients that were refined separately for each tower. However, as an operational gust forecast tool, we need the scheme to work skillfully in a more regional fashion. Therefore, we will evaluate forecast skill by employing the coefficients computed at MM tower for CE and RM, and JI's model for VA (coefficients computed with two year of data, and skill computed in other tower also with two years data), these matchups having been selected based on comparisons of weather regimes and diurnal cycles.

5. Examples of convective events

As noted above, convective activity is frequent in South America (Zipser et al., 2006). In particular, the subtropical region of South America is a favored location for intense thunderstorms associated with MCSs and thus is highly susceptible to heavy rainfall (Ungerovich and Barreiro, 2019). Their temporal and spatial distributions suggest that MCSs over this area are likely connected to certain synoptic and mesoscale processes favorable for their development. Specifically, the peak of MCS activity in Paraguay, northern Argentina, and southern Brazil during the summer is indicative of reduced static stability common during this time of year.

The literature describes two different synoptic patterns conducive to the development of deep convection in the southern region of South America. One is associated with deep convection activity that starts in central Argentina and west of Uruguay. This pattern is due to extremely unstable local conditions caused by positive temperature anomalies and evaporation (Ungerovich and Barreiro, 2019). After initiation, convective systems move eastward, reaching Uruguay a day or two later. An important ingredient in this pattern is a continental scale gyre (the South Atlantic subtropical high) that transports moisture westward from the tropical Atlantic Ocean to the Amazon basin. The aforementioned SALLJ is the regional strengthening of this gyre to the east of the Andes Mountains, with the strongest winds being observed in Bolivia near Santa Cruz de la Sierra. The SALLJ can transport considerable moisture from the Amazon to the La Plata basin (Virji, 1981; Paegle et al., 1987; Vera et al., 2006).

The second pattern involves the migration of synoptic-scale extratropical cyclones as described by (Carlson, 1991) and (Bluestein, 1992). Climatologies demonstrate that cyclones are ubiquitous in South America (e.g., Reboita et al., 2010). In particular, subtropical cyclones are frequent between 20° and 35°S latitude in weak baroclinic environments associated with deep moist convection (Hart, 2003; Evans and Guishard, 2009; Guishard et al., 2009), sometimes presenting mixed characteristics of extratropical and tropical cyclones. The River Plata Basin is a region of development of low pressure systems that cross over Argentina and Uruguay and move towards the Atlantic Ocean (Reboita et al., 2010)). Cold fronts associated with these systems advance over Uruguay, interacting with the warm and moist air transported towards Uruguay via a semi-permanent high pressure system located over the Atlantic Ocean (Garreaud, 2009). The collision of these two air masses triggers convection over the region under study.

Examples of convective activity in the Uruguay region from two sets of GOES-13 imagery (cf. Porrini et al., 2019) are shown in Fig. 4 (04–05 February 2017) and 5 (18–19 August 2017). Following (Gutiérrez and Fovell, 2018), we will define a large gust as that exceeding 15 m/s at hub height, as that value not only often produces the maximum nominal power for commercial wind turbines (Astolfi et al., 2018; Gallego-Castillo et al., 2015) but also resides at the lower range of "cut-out" speeds at which turbines can abruptly stop. As indicated above, as a necessary but not sufficient condition, we will identify potential convective gust situations as when and where the vertically-integrated rainwater mixing ratio equals or exceeds 0.0003 kg_{H2O}/kg_{air} in the WRF simulations for a given location and time, and use that to activate the Nakamura scheme. In Figs. 6 and 7, and Figs. 8 and 9 we present observed and forecasted gusts (at left) and q_r^a forecasts (at right) for the five towers considered herein, derived from simulations using the Bretherton-Park and MYJ PBL schemes, respectively, although they yielded similar results. These figures illustrate both the successes and continuing limitations of this approach.

Overall, it is noted that observed gusts (red lines) intermittently reached but barely exceeded the large gust threshold (dashed horizontal magenta lines). The Gutiérrez–Fovell (G–F) parameterization (superimposed black lines) was generally successful in predicting which side of the gust threshold the observations would fall, but it clearly missed the large gust events at CE on 04 February 2017 between (local times of) 12:00 and 18:00 (Fig. 4) and on 19 August 2017 between 06:00 and 12:00 (Fig. 5), which satellite, radar, and other data indicate were very

Table 2
Number of hourly instances at each station for which q_r^a exceeds the identified threshold between 01/06/2016 and 31/05/2018, which were used for the best fit estimation of the α and β parameters in the Nakamura model.

	CE	JI	MM	RM	VA
MYJ	388	655	496	434	596
Bretherton-Park	336	566	428	383	545

Table 3
α and β parameters for the Nakamura model, minimizing the mean absolute error for convective gusts during training period from 01/06/2016 to 31/05/2018.

	MYJ/Bretherton-Park	
	α	β
CE	0.48/0.49	0.93/0.95
JI	0.47/0.64	0.93/0.89
MM	0.52/0.33	1.03/0.98
RM	0.33/0.19	1.12/1.04
VA	0.73/0.81	0.80/0.83

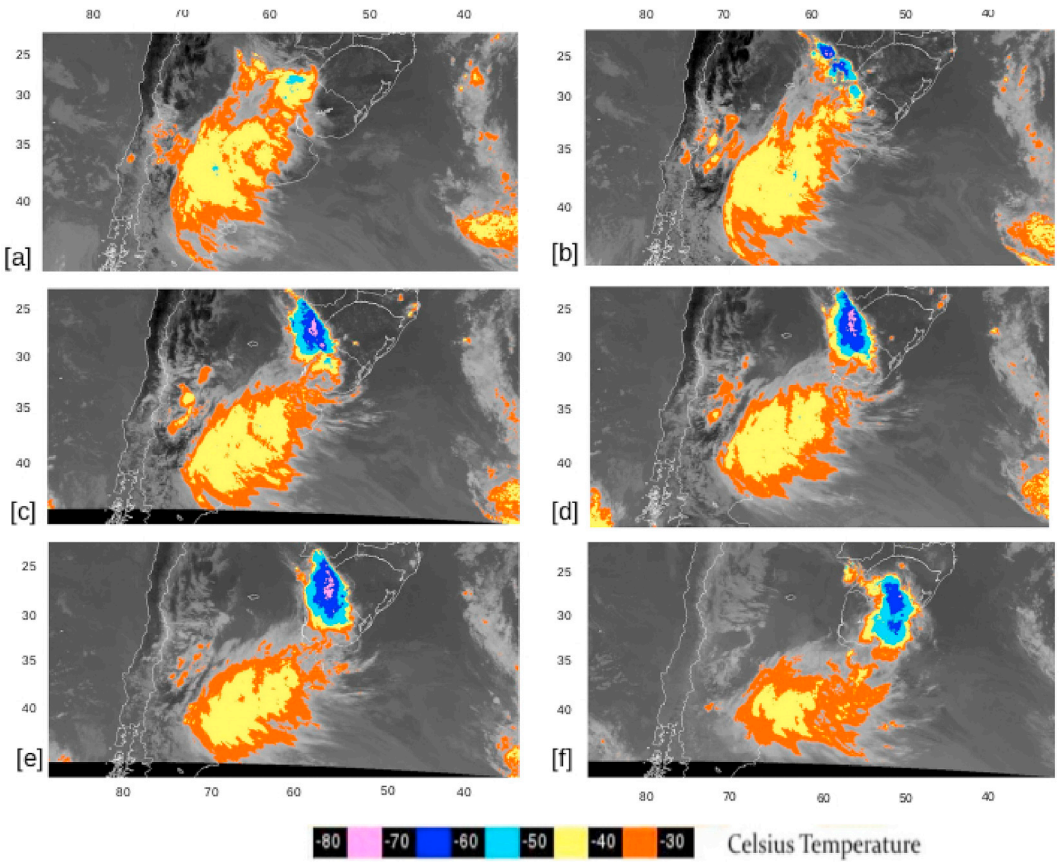

Fig. 4. Set of GOES-13 satellite images for the 04–05 February 2017 convective event, for a) 15:00, b) 18:00, c) 20:00, d) 21:00, and e) 22:00 on 04 February, and f) 02:00 on 05 February, all hours representing local time.

likely related to thunderstorms. During those intervals, the Nakamura parameterization was sporadically activated as predicted rain water mixing ratios exceeded the threshold value (dashed horizontal green lines, at right), providing the gust forecasts indicated by the green dots (at left). For the August case (Figs. 7 and 9), the Nakamura model predicted a large gust closer to the event onset with MYJ, although both methods missed the event's first large gust. Simulated precipitation did not last long at CE, but by the time it ended, the G–F model was providing accurate warnings. The Nakamura model was occasionally activated at the other sites as well; the Nakamura parameterization did not provide different forecasts when active than the G–F was already making in both PBL schemes.

The February event (Figs. 6 and 8) helps illustrate that accuracy also depends on developing convection at the right times and places, which can be challenging for the model. Convective activity did occur in the simulation and warn about large gusts at CE, but several hours after its actual occurrence. This is why the Nakamura forecasts were more successful for the August case than for the February event – the representation of convection was better. Additional skill would be obtained from employing a more sophisticated modeling approach, particularly involving rapid cycling and the assimilation of radar data as is done by the High Resolution Rapid Refresh (HRRR; Benjamin et al., 2016) model in the United States. These examples serve as a demonstration that gust forecast skill enhancement can be realized by adding a convective component to the G–F model.

While there were some differences between simulations using the two PBL schemes, especially with respect to the timing of individual convective events as found in the highlighted February and August 2017 cases, our results suggest that model performance was not significantly influenced by the choice of the boundary layer parameterization.

6. Analysis of results - wind gust alarms

We recognize that coefficients computed with other tower data will reduce the skill for both gust models but this approach is a better representation of a real operational forecast model, that have the goal of forecast gust in an extended region. Furthermore, reflecting the temporally isolated and brief nature of convective gusts, we will only compare observed and simulated winds and gusts occurring within a 1-h interval. As demonstrated in (Gutiérrez and Fovell, 2018), this will also constrain skill. Finally, we will evaluate a combination of the G–F and Nakamura forecasts consisting of the larger value generated by the two approaches; this will be called the combined model.

Figs. 10–12 show scatterplots of observed gusts (g) vs. gust forecasts (g_f) derived from WRF simulations employing the Bretherton–Park planetary boundary layer scheme, for G-F, Nakamura, and the combined model. These and remaining plots focus solely on observations categorized as convective owing to being associated with forecasts of column rainwater exceeding the pre-selected threshold for towers CE, RM, and VA, respectively. This categorization assumes that the model is correctly creating storm events, which is necessary for our study as the electric utility depends on our operational model forecasts of convective activity, and our interest is in anticipating large gusts the G–F model may be missing. The left panels summarize forecast error frequency while forecasted and observed gusts are directly compared at right. With the large gust alarm target of 15 m/s, indicated by the horizontal magenta line, a red dot above the line represents a true alarm (TA), a blue dot above it means a false alarm (FA), and red dots below horizontal magenta line are missed events (MEs).

The top panels of Figs. 10–12 reveal there is skill in the G–F gust forecasting approach, even in situations the model associates with

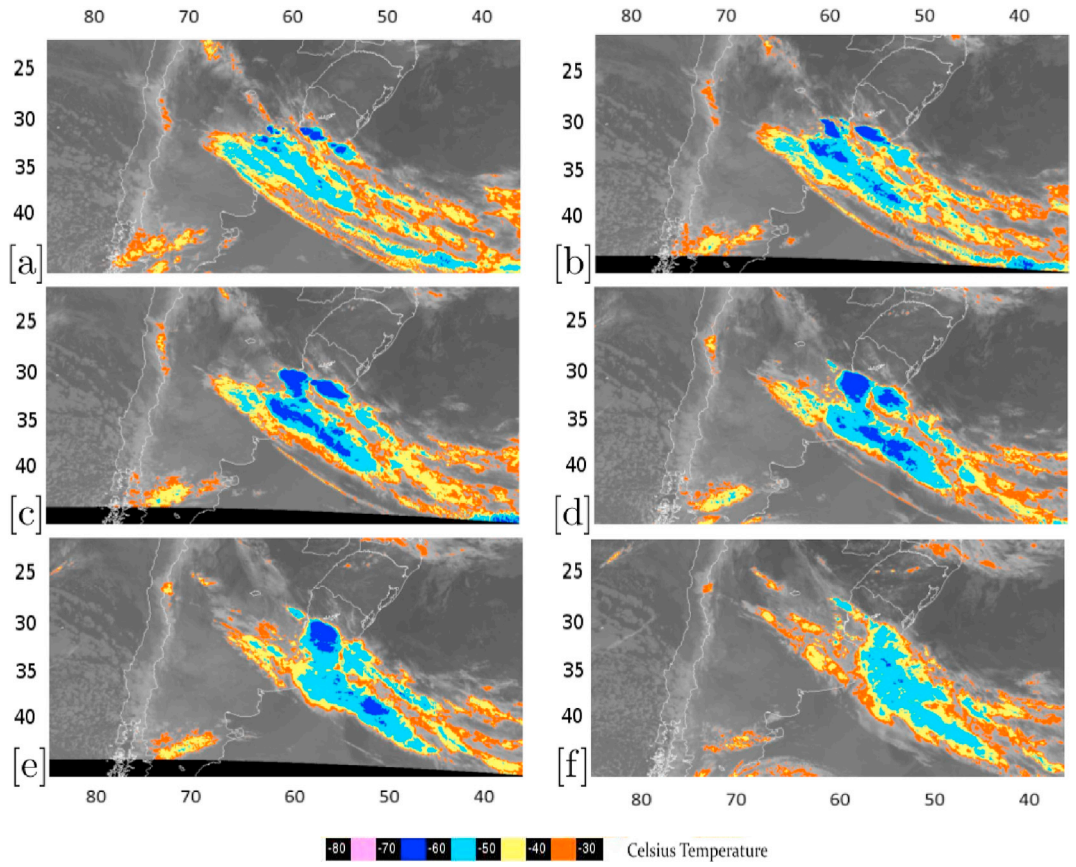

Fig. 5. Set of GOES-13 satellite images for the 18–19 August 2017 convective event, for a) 06:00, b) 07:00, c) 08:00, d) 09:00, e) 10:00, and f) 12:00, all hours representing local time on 19 August.

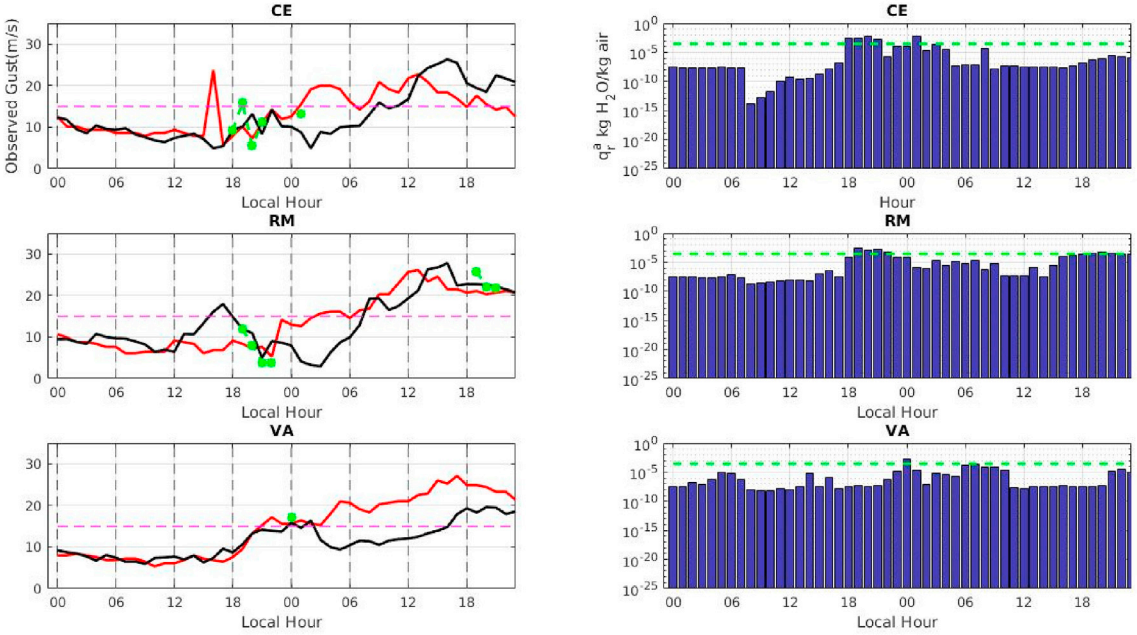

Fig. 6. For the convective event of 04–05 February 2017, the left column displays observed tower-top gusts (red lines, m/s) at CE, RM, and VA towers (see Table 1), with the dashed magenta horizontal lines indicating the 15 m/s large gust threshold, along with Gutiérrez–Fovell (black curve) and Nakamura (green dots) gust forecasts made from simulations utilizing the Bretherton–Park PBL scheme. The right column with vertical axis logarithmic scale indicates forecast q_r^a for each tower location, with the dashed green horizontal lines representing the $q_r^a \geq 0.0003\ \mathrm{kg}_{H2O}/\mathrm{kg}_{air}$ threshold. (For interpretation of the references to colour in this figure legend, the reader is referred to the Web version of this article.)

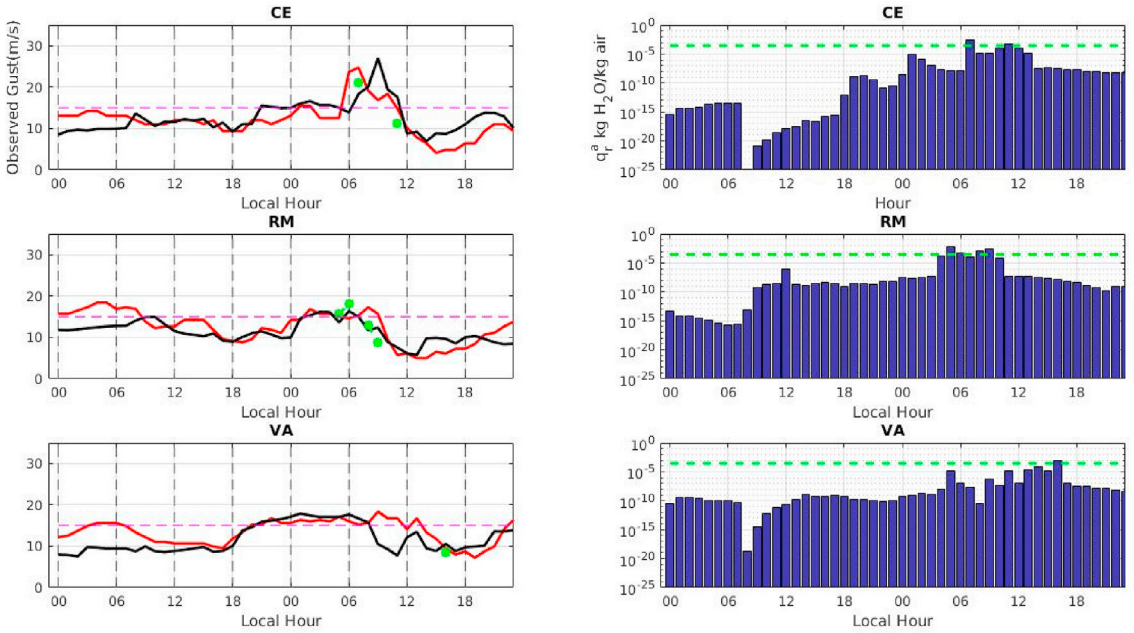

Fig. 7. As in Fig. 6 Bretherton–Park PBL scheme for the 18–19 August 2017 case.

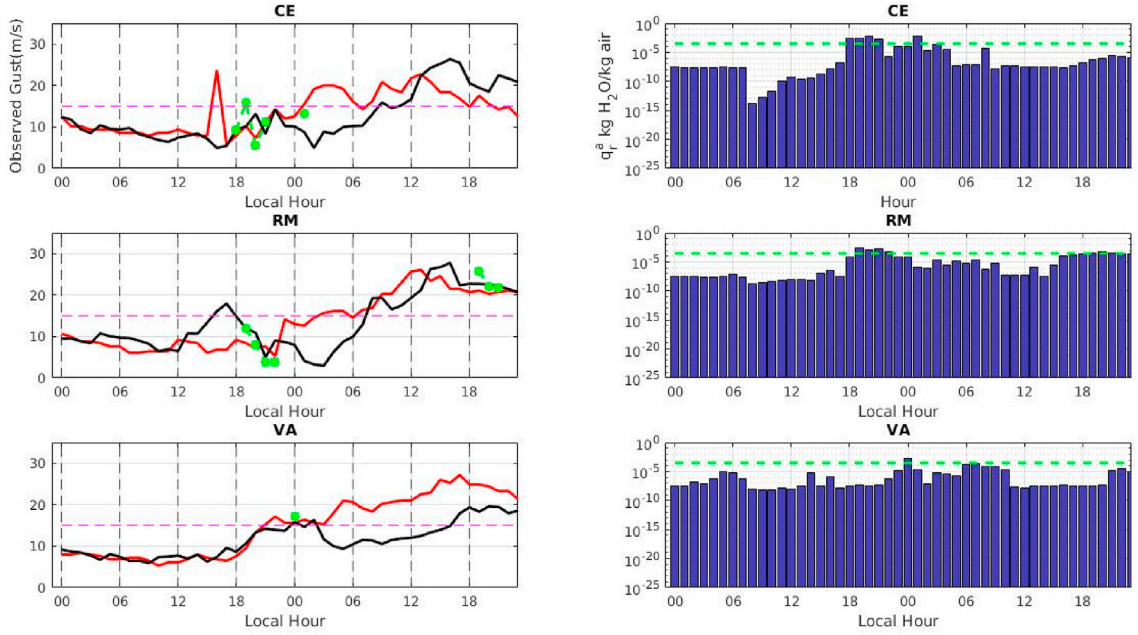

Fig. 8. As in Fig. 6 MYJ PBL scheme for 04–05 February 2017 case.

precipitation. There is a general tendency to predict larger winds when faster values are actually observed, and the coefficient of variation (R^2) is 0.32 for CE, 0.37 for RM and 0.13 for VA. While it is desirable to skillfully predict the specific magnitudes of impending gusts, in practice it suffices to categorize them accurately, and many of the observations that were below the large threshold (the blue dots) are correctly classified (those residing in the lower left quadrant), and few fall into the upper left quadrant, which represents false alarms. At CE tower, the ratio of true alarms to large gust incidents (the true alarm rate,[1] or TAR) is 64% for the Bretherton–Park simulations, while the false discovery rate (FDR) is 45% (Table 4). FDR, the fraction of all large gust forecasts that are in error, is preferred in this application as the number of non-large gust observations and predictions is very large, which makes the false alarm rate (FAR) deceptively small.[2]

A fair fraction of the large gust observations (the red dots), however, are missed events, residing in the lower right quadrant. Bearing in mind that these are observations that the *model* identifies as possibly convective, we hope to capture these gusts by more directly computing convective gust potential, in this case with the Nakamura approach. The Nakamura forecasts are shown in the middle rows of Figs. 10–12. For this

[1] TAR is also referred to as the Probability of Detection, or POD.

[2] Note that TAR and FDR do not sum to 100%.

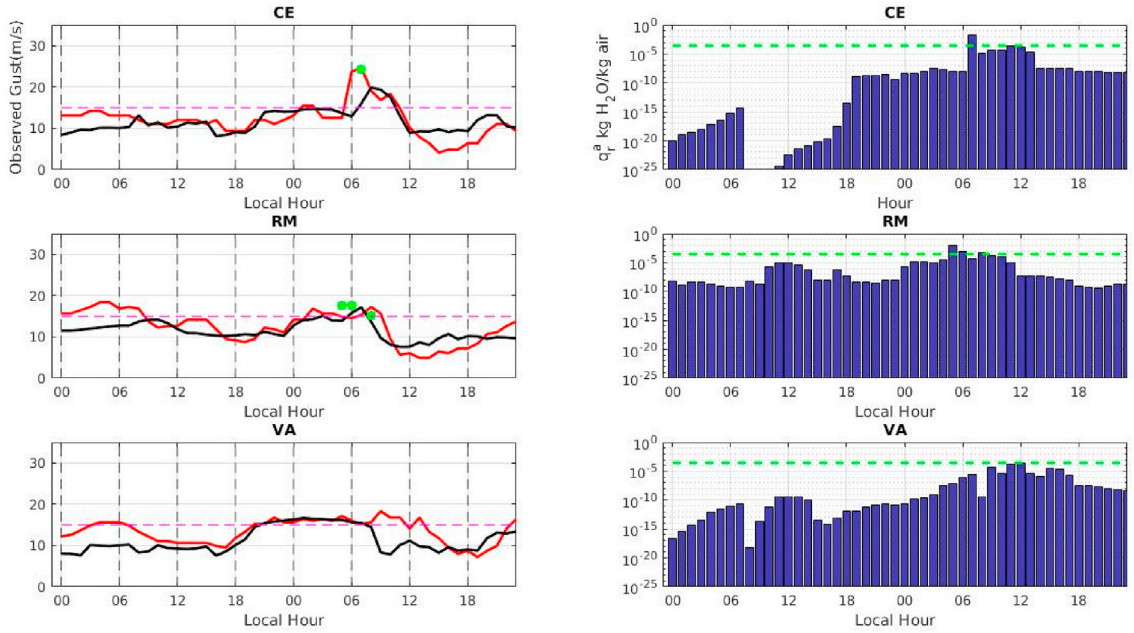

Fig. 9. As in Fig. 6 MYJ PBL scheme for the 18–19 August 2017 case.

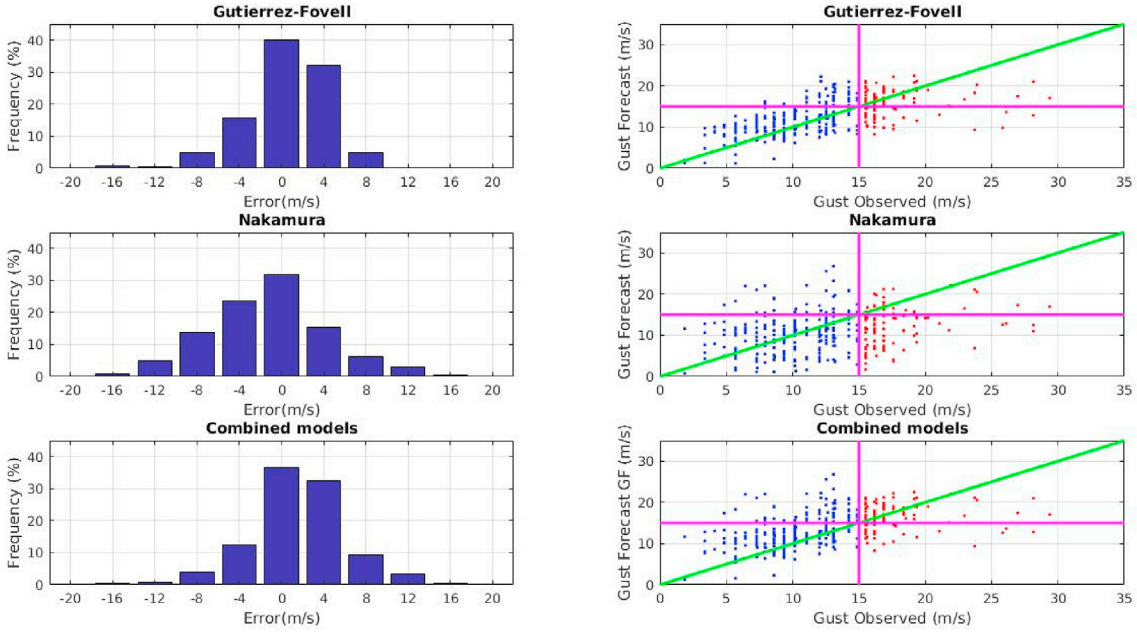

Fig. 10. Histograms of gust forecast error frequency (at left) and scatterplots of observed (g) vs. forecasted (g_f) gusts (at right) at CE tower between 01/06/2016 and 31/05/2018 for model-identified convective cases ($q_r^a \geq 0.0003$ kg_{H2O}/kg_{air}) utilizing simulations made with the Bretherton–Park parameterization. Top row: Gutiérrez–Fovell, middle row: Nakamura, bottom row: combined gust model. In the scatterplots, blue and red dots indicate observed gusts below and above 15 m/s, respectively, the green line represents $g = g_f$, and the magenta vertical and horizontal lines represent observed and forecast values of $15 m/s$, respectively. (For interpretation of the references to colour in this figure legend, the reader is referred to the Web version of this article.)

approach, TARs range from 30 to 46% for the Bretherton–Park runs (Table 4), and are smaller than the corresponding FDRs, which indicates that this method is not very competitive, at least in isolation and in this implementation, even though it was developed specifically for convective wind events.

A combination of the two models, however, can result in improved forecasts, especially at locations where G–F skill is relatively low. At VA tower (Fig. 12), for example, the G–F model only achieved a TAR of 46% in the Bretherton–Park runs (and was even lower with MYJ). However, this was Nakamura's best-performing site, and the combining the models elevated the TAR to 67% at the a relatively small cost of additional false detections. Part of the issue at the inland VA tower is the use of coefficients developed for JI, which is along the coast. That said, coefficients developed for the other towers fared no better (not shown). It turns out that gust incidents coincident with precipitation are particularly common at VA (70% more frequent than at the other inland tower, CE; Table 4), and it is in these situations that the Nakamura approach adds the most value to the combined model.

The Richardson number Ri is a ratio of vertical stability and wind shear. Earlier, we mentioned that the G–F model includes an empirically-

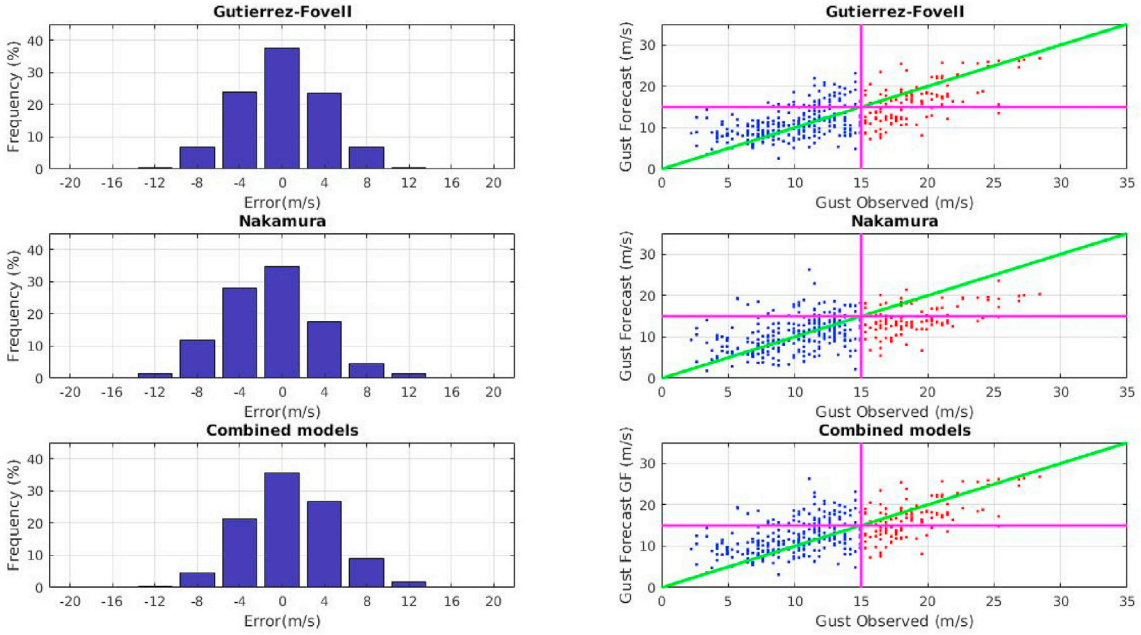

Fig. 11. As in Fig. 10 but for RM tower.

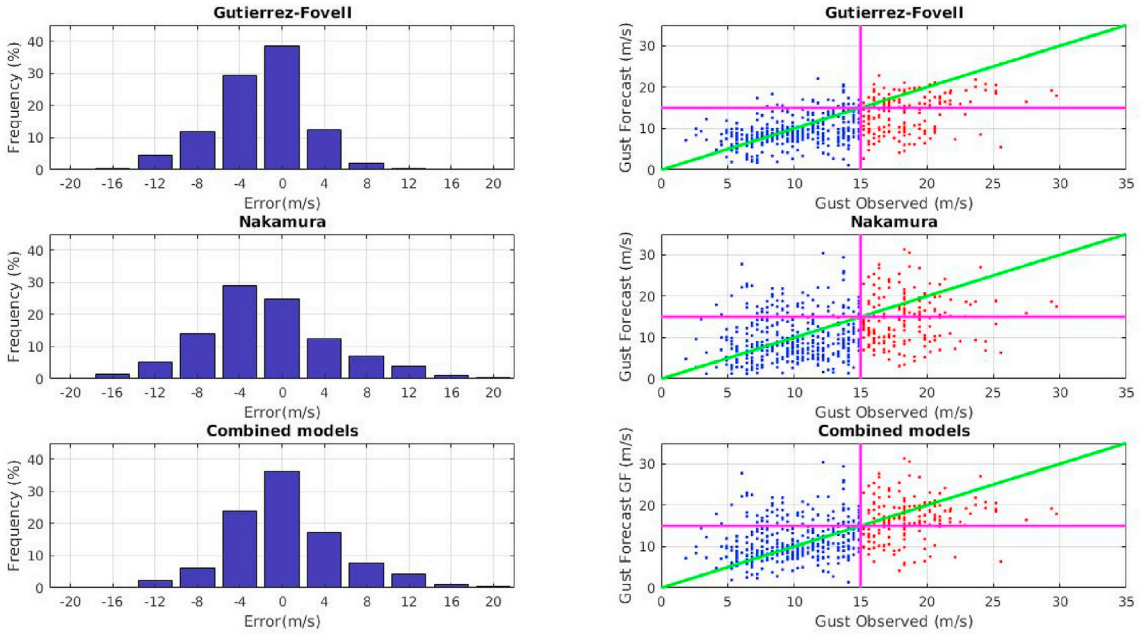

Fig. 12. As in Fig. 10 but for VA tower.

tuned gust forecast enhancement (S_{Ri}) when the surface layer stability is near-neutral ($Ri^{\sim} 0$) (Gutiérrezand Fovell, 2018) showed that the largest observed gusts occurred when tower observations indicated the presence of near-neutral surface layers, especially if the shear was sufficiently large and the PBL was not too deep. Table 5 shows the percentage of all TA cases predicted by the G–F model that occurred when the S_{Ri} correction was applied. It is clear that, at all three towers, nearly all true alarms occurred when the *model* was predicting near-neutral surface layer stability.

7. Conclusion

Gust forecasting is important for electric utilities with high levels of wind power participation, such as the Uruguayan system. Uruguay is also prone to intense storms, so it is important for gust parameterizations employed here also to be capable of anticipating high winds associated with convective activity. We have examined the ability of a recently-developed gust parameterization due to (Gutiérrez and Fovell, 2018) to identify high wind events observed during hours that may have occurred along with thunderstorms. Observations were collected at several towers distributed across the country, which included winds and gusts at 100 m AGL (approximately turbine hub height). Convective activity was diagnosed from numerical weather prediction models via the simulated presence of vertically-integrated rain water exceeding a selected threshold (q_r^a). Satellite imagery was employed to confirm the model predictions of convective activity could be accurate. Simulations, data, and imagery were made or collected over a period of two full years.

As the (Gutiérrez and Fovell, 2018), or G–F, algorithm was developed

Table 4
True alarm rate (TAR) and false detection rate (FAR) statistics for VA, CE, and RM tower gust forecasts for hourly incidents identified by the model as potentially convective for which observations exceeded the large gust threshold of 15 m/s, for MYJ and Bretherton–Park PBL schemes.

Tower	VA	CE	RM
Number convective events, observed gusts $g > 15$ m/s (MYJ/B–P runs)	173/ 170	102/ 101	148/ 122
MYJ/B–P TAR Gutiérrez–Fovell	35/ 46%	60/ 64%	55/ 58%
MYJ/B–P TAR Nakamura	42/ 46%	24/ 30%	40/ 37%
MYJ/B–P TAR Combined	54/ 67%	65/ 68%	61/ 62%
MYJ/B-P FDR Gutiérrez–Fovell	30/ 32%	44/ 45%	35/ 38%
MYJ/B-P FDR Nakamura	54/ 47%	65/ 61%	43/ 40%
MYJ/B-P FDR Combined	49/ 40%	52/ 51%	42/ 47%

Table 5
Percentage of all true alarm (TA) cases, for hourly incidents identified by the model as potentially convective, occurring with the G–F model when the S_{Ri} correction was applied. Data for three towers (VA, CE, and RM) and two model configurations are listed.

PBL scheme used	VA	CE	RM
MYJ	98%	100%	98%
B–P	99%	91%	98%

for generic, non-convective gusts, we also examined a scheme discussed in (Nakamura et al., 1996). That approach attempts to model the momentum of parcels transported towards the surface by downdraughts. The Nakamura model was activated by the aforementioned q_r^a threshold, which was selected empirically to be small enough to activate in the presence of precipitation but sizable enough to discourage false positives. Forecasts were made using both schemes for hourly gust events identified by the model as potentially convective along with a third forecast (the combined model) representing the larger of the two gust predictions. Our analysis herein focused solely on these identified convective events.

We demonstrated herein that G–F scheme has useful skill in delineating between larger and smaller gusts during identified precipitation events, even though it does not attempt to specifically account for the physics of convectively-driven gusts. Skill varied among the towers, with the true alarm rate being highest and lowest at Colonia Eulacio (CE) and Valentines (VA), respectively, being the two inland sites (Fig. 1). Fortuitously, the Nakamura approach proved best at the VA site, and outperformed G–F there. At all sites, combining the two gust forecasts resulted in the highest true alarm rate, albeit with some increase in false detections.

This is a practical, operational problem, one in which skill is potentially limited by the numerical model's success in placing storms at the right places and times. This is challenging even for the best operational models. Success will also depend on physical parameterizations used for microphysics and cumulus convection although we reported only on the planetary boundary layer sensitivity herein. This is a demonstration project and we believe the results are encouraging. Deployment of the combined gust model in an operational environment with high-quality numerical models, ensemble with different parameterizations schemes, employing rapid cycling and radar data assimilation will provide even better guidance.

CRediT authorship contribution statement

Alejandro Gutiérrez: Conceptualization, Methodology, Software, Validation, Formal analysis, Investigation, Resources, Writing - original draft, Writing - review & editing, Visualization, Supervision, Project administration, Funding acquisition. **Claudio Porrini:** Software, Validation, Formal analysis, Investigation, Data curation, Visualization. **Robert G. Fovell:** Conceptualization, Validation, Formal analysis, Investigation, Writing - original draft, Writing - review & editing, Visualization, Supervision.

Acknowledgements

The authors wish to acknowledge the Administración Nacional de Usinas y Trasmisiones Eléctricas (UTE) for providing access to wind data; the Cluster FING-UdelaR for facilitating the development of numerical simulations. Claudio Porrini and Alejandro Gutiérrez was supported by FSDA-1-2017-1-143997 and CSIC–I + D-Gust-WRF Robert Fovell was supported by NSF 1450195.

References

Astolfi, D., Castellani, F., Terzi, L., 2018. Wind turbine power curve upgrades. At. Energ. 11 (5), 1300.
Beljaars, A.C.M., 1987. The influence of sampling and filtering on measured wind gusts. J. Atmos. Ocean. Technol. 4, 613–626.
Berbery, E.H., Collini, E.A., 2000. Springtime precipitation and water vapor flux convergence over southeastern South America. Mon. Weather Rev. 128, 1328–1346.
Bluestein, H.B., 1992. Synoptic-dynamic Meteorology in Midlatitudes, Volumes I and II. Oxford University Press, New York.
Benjamin, S.G., Brown, J.M., Smirnova, T.G., 2016. Explicit precipitation-type diagnosis from a model using a mixed-phase bulk cloudrecipitation microphysics parameterization. Weather Forecast. 31, 60919.
Bretherton, C.S., Park, S., 2009. A new moist turbulence parameterization in the Community Atmosphere Model. J. Clim. 22, 3422–3448.
Brooks, H.E., Doswell, C.A., Kay, M.P., 2003. Climatological estimates of local daily tornado probability for the United States. Weather Forecast. 18, 626–640.
Cao, Y., Fovell, R.G., 2016. Downslope windstorms of san diego county. Part I: a case study. Mon. Weather Rev. 144, 529–552.
Cao, Y., Fovell, R.G., 2018. Downslope windstorms of San Diego County. Part II: physics ensemble analyses and gust forecasting. Weather Forecast. 33, 539–559.
Carlson, T.N., 1991. Mid-latitude weather systems. Am. Meteorol. Soc.
Cazes-Boezio, G.H., Robertson, A.W., Mechoso, C.R., 2003. Seasonal dependence of ENSO teleconnections over South America and relations with precipitation in Uruguay. J. Clim. 16, 1159–1176.
Chen, F., Dudhia, J., 2001. Coupling an advanced land-surface/hydrology model with the Penn State/NCAR MM5 modeling system. Part I: model description and implementation. Mon. Weather Rev. 129, 569–585.
Choi, E.C.C., Hidayat, F.A., 2002. Gust factors for thunderstorm and non-thunderstorm winds. J. Wind Eng. Ind. Aerod. 90, 1683–1696.
Dial, G.L., Racy, J.P., Thompson, R.L., 2010. Short-term convective mode evolution along synoptic boundaries. Weather Forecast. 25, 1430–1446.
Dudhia, J., 1989. Numerical study of convection observed during the winter monsoon experiment using a mesoscale two-dimensional model. J. Atmos. Sci. 46, 3077–3107.
Evans, J., Guishard, M.P., 2009. Atlantic subtropical storms. Part I: diagnostic criteria and composite analysis. Mon. Weather Rev. 137, 2065–2080.
Friederichs, P., Gober, M., Bentzien, S., Lenz, A., Krampitz, R., 2009. A probabilistic analysis of wind gusts using extreme value statistics. Meteorol. Z. 18, 615–629.
Gallego-Castillo, C., Cuerva-Tejero, A., Lopez-Garcia, O., 2015. A review on the recent history of wind power ramp forecasting. Renew. Sustain. Energy Rev. 52, 1148–1157.
Garreaud, R.D., Vuille, M., Compagnucci, R., Marengo, J., 2009. Present-day south american climate. Palaeogeogr. Palaeoclimatol. Palaeoecol. 281 (3–4), 180–195.
Gray, M.E.B., 2003. The use of a cloud resolving model in the development and evaluation of a probabilistic forecasting algorithm for convective gusts. Meteorol. Appl. 10, 239–252.
Guishard, M.P., Evans, J.L., Hart, R.E., 2009. Atlantic subtropical storms, Part II: climatology. J. Clim. 22, 3574–3594.
Gutiérrez, A., Fovell, R.G., 2018. A new gust parameterization for weather prediction models. J. Wind Eng. Ind. Aerod. 177, 45–59.
Hart, R.E., 2003. A cyclone phase space derived from thermal wind and thermal asymmetry. Mon. Weather Rev. 131, 585–616.
Hu, W., Letson, F., Barthelmie, R.J., Pryor, S.C., 2018. Wind gust characterization at wind turbine relevant heights in moderately complex terrain. J. Appl. Met. Clim. 57–7, 1459–1476.
IEC. 61400-61412. First edition. 1998-02. Wind Turbine Generator Systems. Part 12: Wind Turbine Power Performance Testing.
Janjic, Z.I., 1994. The step-mountain eta coordinate model: further developments of the convection, viscous sublayer, and turbulence closure schemes. Mon. Weather Rev. 122, 927–945.
Kain, J.S., 2004. The Kain-Fritsch convective parameterization: an update. J. Appl. Meteor. Climatol. 43, 170–181.
Kain, J.S., Fritsch, J.M., 1990. A one-dimensional entraining/detraining plume model and its application in convective parameterization. J. Atmos. Sci. 47, 2784–2802.

Knigge, C., Raasch, S., 2019. Improvement and development of one- and two-dimensional discrete gust models using a large-eddy simulation model. J. Wind Eng. Ind. Aerod. 153, 46–59.
Letson, F., Pryor, S.C., Barthelmie, R.J., Hu, W., 2018. Observed gust wind speeds in the coterminous United States, and their relationship to local and regional drivers. J. Wind Eng. Ind. Aerod. 173, 199–209.
Lin, Y.L., Farley, R.D., Orville, H.D., 1983. Bulk parameterization of the snow field in a cloud model. J. Clim. Appl. Meteorol. 22, 1065–1092.
Marengo, J.A., Soares, W.R., Saulo, C., Nicolini, M., 2004. Climatology of the Low-Level Jet East of the Andes as Derived from the NCEP–NCAR Reanalyses: Characteristics and Temporal Variability.
Mellor, G.L., Yamada, T., 1974. A hierarchy of turbulence closure models for planetary boundary layers. J. Atmos. Sci. 31, 1791–1806.
Mellor, G.L., Yamada, T., 1982. Development of a turbulence closure model for geophysical fluid problems. Rev. Geophys. Space Phys. 20, 851–875.
Mlawer, E.J., Taubman, S.J., Brown, P.D., Iacono, M.J., Clough, S.A., 1997. Radiative transfer for inhomogeneous atmosphere: RRTM, a validated correlated-k model for the long-wave. J. Geophys. Res. 102, 16663–16682.
Mo, K.C., Paegle, J.N., 2001. The Pacific–South American modes and their downstream effects. Int. J. Climatol. 21, 1211–1229.
Mulholland, J.P., Nesbitt, S.W., Trapp, R.J., Rasmussen, K.L., Salio, P.V., 2018. Convective storm life cycle and environments near the sierras de C órdoba, Argentina. Mon. Weather Rev. 146, 2541–2557.
Nakamura, K., Kershaw, R., Gait, N., 1996. Prediction of near-surface gusts generated by deep convection. Meteorol. Appl. 3 (2), 157–167.
Nesbitt, S.W., Cifelli, R., Rutledge, S.A., 2006. Storm morphology and rainfall characteristics of TRMM precipitation features. Mon. Weather Rev. 134, 2702–2721.
Paegle, J., Zhang, C.D., Baumhefner, D.B., 1987. Atmospheric response to tropical thermal forcing in real data integrations. Mon. Weather Rev. 115, 2975–2995.
Porrini, C., Gutiérrez, A., Fovell, R.G., 2019. Wind gust models comparison in convective events. In: 15th International Conference on Wind Engineering, Beijing, China.
Rasmussen, K.L., Houze, R.A., 2011. Orogenic convection in subtropical South America as seen by the TRMM satellite. Mon. Weather Rev. 139, 2399–2420.
Reboita, M.S., da Rocha, R.P., Ambrizzi, T., Sugahara, S., 2010. South Atlantic ocean cyclogenesis climatology simulated by regional climate model (RegCM3). Clim. Dynam. 35, 1331–1347. https://doi.org/10.1007/s00382-009-0668-7.
Saulo, C., Nicolini, M., Chou, S.C., 2000. Model characterization of the South American low-level flow during the 1997–98 spring–summer season. Clim. Dynam. 16, 867–881.
Shu, Z.R., Li, Q.S., He, Y.C., He Chan, P.W., 2015. Gust factors for tropical cyclone,monsoon and thunderstorm winds. J. Wind Eng. Ind. Aerod. 142, 1–14.
Skamarock, W.C., co-authors, 2008. A Description of the Advanced Research WRF Version 3. NCAR/TN 475+STRNCAR Tech. Note.
Stucki, P., Dierer, S., Welker, C., Gomez-Navarro, J.J., Raible, C.C., Martius, O., Brönnimann, S., 2016. Evaluation of downscaled wind speeds and parameterised gusts for recent and historical windstorms in Switzerland. Tellus A 68, 31820.
Ungerovich, M., Barreiro, M., 2019. Dynamics of extreme rainfall events in summer in southern Uruguay. Int. J. Climatol.
UTE Map of Installed Power Capacity in Uruguay, July of 2019. www.ute.com.uy.
Vera, C., Baez, J., Douglas, M., Emmanuel, C.B., Marengo, J., Meitin, J., Nicolini, J., Nogues-Paegle, J., Paegle, J., Penalba, O., Salio, P., Saulo, Silva Dias, C., Dias, P.S., Zipser, E., 2006. the South American low-level jet experiment. Bull. Am. Meteorol. Soc. 87, 63–78.
Virji, H., 1981. A preliminary study of summertime tropospheric circulation patterns over South America estimated from cloud winds. Mon. Weather Rev. 109, 599–610.
Wyngaard, J.C., 2004. Toward numerical modelling in the Terra incognita. J. Atmos. Sci. 61, 1816–1826.
Yang, T.H., Tsai, C.C., 2019. Using numerical weather model outputs to forecast wind gusts during typhoons. J. Wind Eng. Ind. Aerod. 188, 247–259.
Zipser, E.J., Cecil, D.J., Liu, C., Nesbitt, S.W., Yorty, D.P., 2006. Where are the most intense thunderstorm on earth? Bull. Am. Meteorol. Soc. 87, 1057–1072.